Published in final edited form as:
Radiology. 2016 February ; 278(2): 430–440. doi:10.1148/radiol.2015142899.

Squamous Cell Carcinoma Xenografts: Use of VEGFR2-targeted Microbubbles for Combined Functional and Molecular US to Monitor Antiangiogenic Therapy Effects

Sarah C. Baetke, M.Sc.[1], **Anne Rix, B.Sc.**[1], **François Tranquart, MD, PhD**[2], **Richard Schneider, PhD**[3], **Twan Lammers, PhD, DSc**[1], **Fabian Kiessling, MD**[1,*], and **Wiltrud Lederle, PhD**[1]

[1]Department of Experimental Molecular Imaging, Helmholtz Institute for Biomedical Engineering, RWTH Aachen University, Aachen, Germany [2]Bracco Suisse SA, Geneva, Switzerland [3]Merck Serono, Darmstadt, Germany

Abstract

Purpose—To assess the ability of vascular endothelial growth factor receptor type 2 (VEGFR2)-targeted and nontargeted ultrasonography (US) to depict antiangiogenic therapy effects and to investigate whether first-pass kinetics obtained with VEGFR2-targeted microbubbles provide independent data about tumor vascularization.

Materials and Methods—Governmental approval was obtained for animal experiments. Vascularization in response to anti-vascular endothelial growth factor receptor or vehicle-control treatment (n=10/group) in HaCaT-ras A-5RT3 xenografts was longitudinally assessed in mice by means of first-pass kinetics of nontargeted microbubbles (BR1, BR38; Bracco, Geneva, Switzerland) and VEGFR2-targeted microbubbles (BR55; Bracco) before and 4, 7, and 14 days after therapy. VEGFR2 expression was determined 8 minutes after BR55 injection with destruction-replenishment analysis. US data were validated by immunohistochemistry. Significant differences were evaluated with the Mann-Whitney test.

Results—First-pass analysis with BR1, BR38, and BR55 showed similar tendencies toward decreasing vascularization, with a stronger decrease in tumors treated with anti-VEGF antibody. The median signal intensity (in arbitrary units [au]) of anti-VEGF antibody-treated versus control tumors at day 14 was as follows: BR1, 5.2 au (interquartile range [IQR], 3.2 au vs 11.3 au (IQR, 10.0 au), respectively; BR38, 6.2 au (IQR, 3.5 au) vs 10.0 au (IQR, 7.8 au); and BR55, 9.5 au (IQR, 6.0 au) vs 13.8 au (IQR, 9.8 au) (p=0.0230). VEGFR2 assessment with BR55 demonstrated significant differences between both groups throughout the therapy period (median signal intensity of anti-VEGF antibody-treated vs control tumors: 0.04 au [IQR, 0.1 au] vs 0.14 [IQR, 0.08 au], respectively, at day 4, p=0.0058; 0.04 au [IQR, 0.06 au] vs 0.13 au [IQR, 0.09 au] at day 7, p=0.0058; and 0.06 au [IQR, 0.11 au] vs 0.16 au [IQR, 0.15 au] at day 14, p=0.0247).

[*]Corresponding author: Fabian Kiessling, Department of Experimental Molecular Imaging, Medical Faculty, RWTH Aachen University, Pauwelsstraße 30, 52074 Aachen, Germany, Tel: +49 (0)241 80-80116, Fax: +49 (0)241 80-82006, fkiessling@ukaachen.de.

Immunohistochemistry confirmed the lower microvessel density and VEGFR2-positive area fraction in tumors treated with anti-VEGF antibody.

Conclusion—Antiangiogenic therapy effects were detected earlier and more distinctly with VEGFR2-targeted US than with functional US. First-pass analyses with BR55, BR38, and BR1 revealed similar results, with a decrease in vascularization during therapy. Functional data showed that BR55 is not strongly affected by early binding of the microbubbles to VEGFR2. Thus, functional and molecular imaging of angiogenesis can be performed with BR55 within one examination.

Introduction

Angiogenesis, the formation of new blood vessels from pre-existing ones, has been identified as a major hallmark of cancer. It constitutes an essential prerequisite for tumor growth, invasion, and metastasis, enabling tumors to grow beyond a size of 1-2 mm. Angiogenesis has been characterized as a complex, multistep process that involves numerous angiogenic factors and cytokines (1–5).

The most prominent imaging marker of angiogenesis is the vascular endothelial growth factor (VEGF) receptor type 2 (VEGFR2), which is highly up-regulated during the onset of tumor growth (6–8). Because numerous antiangiogenic therapeutic agents either directly bind to the extra- or intracellular domain of VEGFR2 or block its natural ligand VEGF (9), imaging of VEGFR2 at the molecular level constitutes an attractive opportunity to monitor antiangiogenic cancer therapy (10).

Currently, ultrasonography (US) is one of the most commonly used diagnostic imaging modalities in clinical medicine. Gas-filled microbubbles are routinely used to enhance the contrast of tumors and for the functional assessment of vascularization (11,12). In this context, functional assessment includes the visualization of vessels and the quantification of blood velocity, perfusion and relative blood volume (rBV). First-pass analysis of the acquired cine loop data with use of accumulated maximum intensity over time (MIOT) showed a significant correlation with the rBV in tumors (11,13). Several studies strengthen the utility of contrast material-enhanced functional US to quantify antiangiogenic therapy effects on the basis of a significant reduction in rBV in treated tumors compared with untreated ones (11). In addition, the use of molecularly targeted microbubbles at US has emerged as a very suitable method in preclinical settings, allowing noninvasive analysis of tumor angiogenesis and antiangiogenic therapy effects (10–13). Consequently, additional preclinical studies have demonstrated the feasibility of targeting VEGFR2 for the detection of early tumor lesions and antiangiogenic therapy responses (14–18). The specific accumulation of targeted microbubbles at the pathologic site can be assessed by subtracting the US imaging signal after applying a destructive pulse from that before the destructive pulse (11).

Most molecularly targeted US studies targeting VEGFR2 make use of biotinylated antibodies that are connected to the microbubble surface via the biotin-streptavidin complex. These streptavidin-functionalized microbubbles are not recommended for clinical use due to their potential immunogenicity in humans (19–21). To overcome this limitation and to

Europe PMC Funders Author Manuscripts

facilitate clinical application, novel target-specific microbubbles have been developed (eg, BR55 [Bracco Suisse, Geneva, Switzerland], which is a lipopeptide-based, VEGFR2-targeted molecular US contrast agent). In BR55, the targeting ligands are directly incorporated into the microbubble shell, making it potentially suited for clinical translation (12,20).

The purpose of this study was to assess the ability of VEGFR2-targeted and nontargeted US for depicting antiangiogenic therapy effects in subcutaneous HaCaT-ras A-5RT3 tumor xenografts and to investigate whether first-pass kinetics of VEGFR2-targeted microbubbles provide independent data about tumor vascularization.

Materials and Methods

The US contrast agents (BR1, BR38, and BR55) were provided by Bracco Suisse (Geneva, Switzerland), and the anti-VEGF antibody B20-4.1.1 was provided by Merck Serono (Darmstadt, Germany). At the time of submission, one author (F.T.) is an employee of Bracco Suisse and one author (R.S.) is an employee of Merck Serono. Data collection and analysis were performed by authors without an affiliation to Bracco Suisse and Merck Serono. The authors without affiliation to industry (S.C.B., A.R., T.L., F.K., and W.L.) had full control of the data and information.

Cell Culture

The human skin squamous carcinoma cell line HaCaT-ras A-5RT3 was maintained in Dulbecco`s modified Eagle`s medium and GlutaMAX (Life Technologies, Darmstadt, Germany) supplemented with 10% heat-inactivated fetal bovine serum, 1% penicillin-streptomycin, and 200 μg/ml geneticin at 37° C and 5% CO_2.

Cancer Xenografts

All experiments were approved by the governmental review committee on animal care. HaCaT-ras A-5RT3 cells ($2x10^6$) were subcutaneously injected into the right flank of 40 female CD1 nude mice (Charles River, Sulzfeld, Germany). Tumor growth was monitored regularly with caliper measurements. Tumor volumes were calculated by using the formula: $0.52xAxB^2$, where A represents the largest and B the smallest tumor diameter. Furthermore, the animal`s weight was recorded regularly. At a tumor size of 4-5mm, mice were randomized into one of two treatment groups receiving 20 mg per kilogram body weight B20-4.1.1 (B20) (n=10), an antibody targeting both murine and human VEGF that is analogous to Avastin (Merck Serono, Darmstadt, Germany), or a vehicle control (n=10) composed of 10 mmol/L citric acid, 3% (wt/vol) sucrose, 85 mmol/L NaCl and 0.05% (wt/vol) Tween 20 (Sigma Aldrich, St Louis, Mo). The substances were injected intraperitoneally twice per week over a period of 14 days (Fig 1).

Monitoring Treatment Effects of Antiangiogenic Therapy

Therapy monitoring—Therapy monitoring by molecularly targeted US before therapy (day 0) and 4, 7, and 14 days after treatment initiation to determine the effects on tumor vascularization (n=10/group). The animals were sacrificed after the last imaging

examination. Tumors were resected and cryoconserved in Tissue-Tek (Sakara, Zoeterwoude, The Netherlands) for histologic analysis (Fig 1). Furthermore, two groups of five animals were used for histologic validation at therapy days 4 and 7. During all experimental procedures, mice were anesthetized by inhalation of 2% isoflurane in oxygen-enriched air.

US contrast agents—VEGFR2-targeted BR55 microbubbles (Bracco Suisse) were used to investigate VEGFR2 expression and tumor vascularization (12). BR55 was prepared by adding 2 mLof 5% glucose to the vial, resulting in a concentration of $2x10^9$ microbubbles per milliliter. BR55 microbubbles have a mean diameter of 1.5 μm and are characterized by a circulation time of approximately 4 minutes. *In vitro* competitive binding experiments on human umbilical vein endothelial cells demonstrated the high binding specificity of BR55 for VEGFR2 (12). To further rule out a possible interaction between the anti-VEGF antibody B20 and the VEGFR2-targeted BR55 microbubbles, which might prevent microbubble targeting, additional immunofluorescence microscopy of BR55 and B20 mixtures was performed and indicated that the anti-VEGF antibody B20 does not bind to the BR55 microbubbles.

In addition to BR55, tumor vascularization was assessed by using nontargeted, long-circulating BR38 (Bracco Suisse) (22). Before use, 1 mL of saline was added to the vial yielding a concentration of $1x10^9$ microbubbles per milliliter. BR38 microbubbles have a mean diameter of 1.5 μm but are characterized by a circulation time of approximately 10 minutes until the microbubbles are cleared from the blood. Those microbubbles were extensively evaluated in a previous study in our group with respect to their circulation characteristics and ability to assess differences in tumor vascularization in differentially aggressive breast cancer xenografts (23). Furthermore, the short-circulating, clinically approved BR1 microbubbles (Bracco Suisse) were used as nontargeted control microbubbles in 10 animals (five per group). BR1 was prepared by adding 2 mL of saline to the vial yielding a concentration of $5x10^8$ microbubbles per milliliter. BR1 microbubbles have a mean diameter of 2.5 μm and are characterized by a circulation time of less than 3 minutes (19). Each microbubble type was manually injected into the tail vein over approximately 3 seconds (injection volume, 50 μL followed by a 20-μL saline flush. Animals that received all three microbubble types (five per group) were first injected with the short-circulating BR1 microbubbles, followed by injection of BR55 and BR38. In animals being injected with BR55 and BR38 only, BR55 was injected first, followed by BR38.

First pass analysis and molecularly-targeted US—US measurements were performed by using the Vevo2100 small-animal high-spatial-resolution US system equipped with a MS-250 transducer (VisualSonics, Toronto, Ontario, Canada). The “nonlinear contrast mode” was used with a frequency of 18 MHz and a mechanical index of 0.03. For first-pass analysis, cine loops were acquired for 25.5 seconds (10 frames per second, 255 frames in total) starting with the bolus injection of nontargeted BR1 in ten animals (five per group). After complete clearance from the blood, BR55 was injected (10 animals per group). Eight minutes after the injection, a destructive pulse (mechanical index, 0.7) was applied for 1 second to destroy all microbubbles in the imaged tumor slice, and the vascular replenishment of circulating microbubbles was recorded for approximately 15 seconds.

Europe PMC Funders Author Manuscripts

After clearance of BR55 from the blood, nontargeted BR38 microbubbles were administered and their injection was recorded (10 animals per group).

Image analysis—Image analysis was performed by two scientists (S.C.B. and A.R., with 4 and 7 years of experience, respectively). One observer was blinded to the types of microbubbles and experimental groups and confirmed the results. Image analysis was done with preclinical software (Imalytics; Gremse-IT, Aachen, Germany) (24). A region of interest was defined over the whole tumor. To investigate tumor vascularization, the rBV was determined by applying the MIOT postprocessing method to the acquired cine loop data for BR1, BR38, and BR55 (25). MIOT is a postprocessing technique to map trajectories of circulating microbubbles. Each circulating microbubble leads to an increase in the acoustic intensity of the corresponding pixel. A subsequent pixel-by-pixel analysis comparing the current frame with the previous frame registers the increase in acoustic intensity. Throughout the entire cine loop, the highest amplitude of each pixel is preserved. The mean increase within the imaged tumor frame is displayed as the MIOT curve. To assess the amount of bound BR55, the US imaging signal after the destructive pulse was subtracted from that before the destructive pulse (23). To evaluate the median reduction in US imaging signal throughout the therapy period in percentage, the US imaging signal measured before therapy onset for B20-treated and control animals was set to 100% and the median percentage decrease in US imaging signal for therapy days 4, 7, and 14 determined.

Immunohistochemistry

Immunofluorescent staining was performed on 8-μm-thick tumor slices (26). The following primary antibodies were used: a rat antimouse CD31 antibody (1:100; BD Biosciences, Heidelberg, Germany) to detect endothelial cells, a goat antimouse VEGFR2 antibody (1:20; R&D Systems, Wiesbaden, Germany) to assess angiogenic activity, and a biotinylated anti-α-smooth muscle actin (α-SMA) antibody (1:500; Progen, Heidelberg, Germany) to determine vessel maturation. Secondary antibodies were donkey antirat DyeLight 488 (1:350), donkey antigoat Cy-3 (1:250), and streptavidin-Cy-3 (1:350) (all derived from Dianova, Hamburg, Germany). Cell nuclei were counterstained with Hoechst 33258 (1:400; Sigma-Aldrich, Steinheim, Germany).

Fluorescence microscopy was performed by using an *Axio Imager M2* microscope and a high-resolution camera (AxioCam MRm Rev.3; Carl Zeiss Microimaging, Göttingen, Germany) at 200-fold magnification. For each tumor, six images (three from the tumor periphery and three from the center) from two representative tumor slices were analyzed. The scientists who performed the immunohistochemistry analysis were blinded to the experimental groups. To determine vessel density, the area fraction covered by CD31-positive vessels, including the lumina was quantified. The VEGFR2 expression was quantified by determining the VEGFR2-positive area fraction. To determine vessel maturation, a vessel count was performed and the percentage of the number of α-SMA-positive vessels per total number of vessels was calculated. Micrographs were analyzed by using software (AxioVision Rel 4.8, Carl Zeiss Microimaging).

Statistical Analysis

Statistical analysis was performed by using software (GraphPad Prism 5.0; GraphPad Software, San Diego, Calif). Data are presented as medians ± interquartile ranges (IQRs). The nonparametric Mann-Whitney U test was used to assess statistical significance. Furthermore, for each US contrast agent and time course, the statistical results were corrected for multiple comparisons by using the Benjamini-Hochberg false discovery rate method. The correction was performed by using R (version 3.2.0; R Development Core Team, Vienna, Austria). $P < 0.05$ was considered indicative of a significant difference.

Results

Antiangiogenic Therapy with B20 Leads to Significantly Reduced Growth of HaCaT-ras A-5RT3 Tumors

Subcutaneous injection of HaCaT-ras A-5RT3 cells into CD1 nude mice led to palpable tumors from day 7 onwards after inoculation. Fourteen days after tumor cell injection, tumors had reached a size of 4-5 mm in diameter and the antiangiogenic therapy with B20 was initiated (median tumor volume at day 0: 86 mm^3 [IQR, 52.0 mm^3] in B20-treated group and 83 mm^3 [IQR, 65.8 mm^3] in control group). Although control animals showed a constant increase in tumor volume, those treated with B20 showed reduced tumor growth. Six days after therapy onset, differences in tumor volume between B20-treated tumors (median, 131 mm^3 [IQR, 127.8 mm^3]) and control tumors (median, 181 mm^3 [IQR, 206.8 mm^3]) were significant (p=0.0355). These differences remained significant throughout the remaining therapy period. At the end of the therapy period, a significant difference in tumor volume between the B20-treated tumors (median, 137 mm^3 [IQR, 70.7 mm^3]) and control tumors (median, 400 mm^3, [IQR, 371.6 mm^3]) was observed (p=0.0011) (Fig 2).

Assessment of Tumor Vascularization (rBV) with First-Pass Analysis of Nontargeted BR1

Tumor vascularization was assessed with first-pass analysis of BR1 and postprocessing with MIOT (24). Functional US with the clinically approved, short-circulating BR1 microbubbles showed a tendency toward decreasing rBV values in treated and control tumors, with values being lower in B20-treated tumors (Fig 3). In detail, the median US imaging signal decreased from 100% at day 0 (median US imaging signal, 10.2 au [IQR, 14.0 au] in B20-treated group and 15.9 au [IQR, 9.8 au] in control group) to 72% in control tumors (median US imaging signal, 11.3 au [IQR, 10.0 au] and 51% in B20-treated tumors (median US imaging signal, 5.2 au [IQR, 3.2 au]) at therapy day 14. However, differences between both groups were not significant (Fig 3).

Assessment of Tumor Vascularization (rBV) with First-Pass Analysis of Nontargeted BR38

First-pass analysis with BR38 also indicated a trend toward decreasing rBV values with ongoing treatment in both groups. The median rBV was also lower in tumors of B20-treated animals compared with vehicle-treated controls (Fig 4). The median US imaging signal decreased from 100% at day 0 (median US imaging signal, 14.1 au [IQR, 13.4 au] in B20-treated group and 16.9 au [IQR, 7.2 au] in control group) to 44% in control tumors (median US imaging signal, 10.0 au [IQR, 7.8 au]) and 47% in B20-treated tumors (median US

imaging signal, 6.2 au [IQR, 3.5 au]) at therapy day 14. However, differences between both groups were not significant (Fig 4).

Assessment of Tumor Vascularization (rBV) with First-Pass Analysis of BR55

Finally, first-pass analysis with BR55 also showed a tendency toward decreasing values with ongoing therapy in both groups, with a stronger decline in B20-treated animals (Fig 5). The MIOT data were significantly lower in B20-treated compared with control tumors at therapy days 4 (median US imaging signal, 13.1 au [IQR, 3.6 au] in B20-treated group and 18.0 au [IQR, 2.2 au] in control group; p=0.0028) and 14 (median US imaging signal, 9.5 au [IQR, 6.0 au] in B20-treated group and 13.8 au [IQR, 9.8 au] in control group; p=0.0230). The median decrease in US imaging signal of BR55 expressed as a percentage revealed a decrease in US imaging signal from 100% at day 0 (median US imaging signal, 18.6 au [IQR, 15.9 au] in B20-treated group and 21.9 au [IQR, 9.1 au] in control group) to 63% in control tumors (median US imaging signal, 13.8 au [IQR, 9.8 au]) and 51% in B20-treated tumors (median US imaging signal, 9.5 au [IQR, 6.0 au] at therapy day 14.

Assessment of VEGFR2 Expression in HaCaT-ras A-5RT3 Tumor Xenografts with BR55

To assess tumor angiogenesis, molecularly targeted US was performed with VEGFR2-targeted BR55 (Fig 6). The amount of target-bound microbubbles was determined by calculating the difference between the US imaging signal before and after the destructive pulse 8 minutes after microbubble injection (Fig 7).

By therapy day 4, the amount of bound BR55 was significantly lower in B20-treated tumors (median difference, 0.04 au [IQR, 0.1 au]) compared with control tumors (median difference, 0.14 au [IQR, 0.08 au]) (p=0.0058). The amount of bound BR55 in B20-treated tumors remained significantly lower than that in the control tumors throughout the treatment period (day 7: 0.04 au [IQR, 0.06 au] vs 0.13 au [IQR, 0.09 au], respectively, p=0.0058; day 14: 0.06 au [IQR, 0.11 au] vs 0.16 au [IQR, 0.15 au], p=0.0247) (Fig 7).

Ex Vivo Analysis

US data were validated with immunofluorescence analyses of tumor slices. In contrast to rBV measurements with nontargeted BR1 and BR38, immunohistochemical analysis revealed that the microvessel density in tumors after 4 days of treatment with B20 was significantly decreased compared with that in control tumors (median. 4.1% [IQR, 1.2%] vs 7.9% [IQR, 2.9%], respectively; p=0.0079) (Fig 8). At days 7 and 14, the vessel density was also significantly lower in the B20-treated tumors compared with the control tumors (day 7: median, 3.5% [IQR, 0.9%] vs 8.3% [IQR, 1.3%], respectively, p=0.0079; day 14: median, 3.0% [IQR, 1.7%] vs 7.2% [IQR, 4.5%], p=0.0159).

In line with the reduced vessel density, the VEGFR2-positive area fraction was significantly decreased in B20-treated tumors compared with control tumors at day 4 (median, 2.3% [IQR, 1.3%] vs 4.1% [IQR, 1.2%], respectively; p=0.0079), 7 (median, 1.0% [IQR, 0.3%] vs 3.4% [IQR, 1.7%]; p=0.0119), and 14 (median, 0.8% [IQR, 0.4%] vs 1.9% [IQR, 1.2%]; p=0.0079) (Fig 8), confirming the significantly reduced VEGFR2 levels *in vivo* measured with molecularly targeted US.

To investigate the effects of antiangiogenic treatment on vessel maturation, tumor vessels were stained for α-SMA (Fig 9) and the number of α-SMA-positive vessels per total number of vessels was determined. At 4, 7, and 14 days after therapy induction, a comparable percentage of α-SMA-positive vessels was observed in B20-treated and control tumors (day 4: median, 56.5% [IQR, 41.6%; median number of α-SMA-positive vessels per total number of vessels, 12/24] vs 49.3% [IQR, 18.5%; median number of α-SMA-positive vessels per total number of vessels, 9/21]; day 7: median, 43.5% [IQR, 14.3%; median number of α-SMA-positive vessels per total number of vessels, 10/24] vs 56.7% [IQR, 22.5%; median number of α-SMA-positive vessels per total number of vessels, 11/19]; day 14: median, 52.3% [IQR, 19.6%; median number of α-SMA-positive vessels per total number of vessels, 21/34] vs 53.4% [IQR, 30.8%; median number of α-SMA-positive vessels per total number of vessels, 29/53]), indicating no prominent maturation effects on tumor vascularization, neither during growth nor during treatment (Fig 9b).

Discussion

The objective of this study was to assess the ability of VEGFR2-targeted and nontargeted US to depict antiangiogenic therapy effects and to investigate whether first-pass kinetics of BR55 provide independent data about tumor vascularization. Throughout the therapy period, first-pass analyses with BR1, BR38, and BR55 constantly revealed reduced rBV values in B20-treated tumors compared with control tumors, which, however, were not significant for most time points. Conversely, VEGFR2 assessment with BR55 demonstrated significant differences between both groups at all investigated time points, which indicates that VEGFR2-targeted US can enable assessment of antiangiogenic therapy effects earlier than functional US.

This excellent performance of molecularly targeted US in the characterization of neovasculature is consistent with previous results, where molecularly targeted US with BR55 was superior to functional imaging with respect to the differentiation of highly angiogenic from less angiogenic breast tumors (23). Furthermore, molecularly targeted US with BR55 accurately depicted the angiogenic activity in early breast tumors (27) and the malignant, angiogenic conversion of liver dysplasia, which was not possible using functional US with nontargeted microbubbles (28). In agreement with these findings, Bachawal *et al.* (29) demonstrated that molecularly targeted US with BR55 was able to help differentiate between benign and malignant breast tumors with high sensitivity and specificity. Pysz *et al.* (20) longitudinally monitored the antiangiogenic therapy effects of B20 by molecularly targeted US by using BR55 in a human colon cancer xenograft model and observed significant changes in US imaging signal 1 day after the start of therapy. Thus, VEGFR2-targeted US sensitively depicts angiogenic and antiangiogenic activity. Conversely, significant differences between tumor models and early antiangiogneic therapy are often difficult to determine by assessing tumor vascularization (eg, with nontargeted, contrast-enhanced US). This can be explained by the fact that vascularization does not necessarily reflect the angiogenic state of tumors (30). In a tumor with low angiogenesis, slow growth, and high vessel maturation, many functional blood vessels may survive and thus this tumor appears better perfused than a rapidly growing tumor with high angiogenesis but low vessel maturation, where most angiogenic vessels rapidly undergo apoptosis and even do not carry

blood. The latter tumor type typically manifests with only a small angiogenic rim at the periphery of the tumor and a hypovascular core. Vaupel *et al.* (31) already showed many years ago that a significant percentage of tumor vessels are not perfused. This nonperfused vessel fraction consists of either vessels that became thrombotic or small vessels at the angiogenic front. At histologic examination with CD31 staining, these nonfunctional vessels are counted although they are not perfused. It is a limitation of our study that we did not perform isolectin perfusion of animals at the end of the experiments, because it is a useful method for differetiating perfused and nonperfused vessels in histologic specimens when costaining with CD31.

For functional US, we compared BR55 with BR1 and BR38 in the assessment of antiangiogenic therapy effects between B20-treated and control animals at several time points. First-pass analyses with BR1, B38, and BR55 indicated a similar trend in decreasing vascularization in B20-treated and control tumors throughout the therapy period with a stronger decline in B20-treated tumors. This suggests that first-pass analysis with BR55 is not strongly affected by early binding of the microbubbles to VEGFR2 and, therefore, comparable functional results with regard to tumor vascularization can be obtained as with nontargeted microbubbles. In line with this, Tardy *et al.* (19) previously demonstrated that BR55 and the clinical, nontargeted contrast agent BR1 show comparable peak intensities and similar wash-in phases after injection. These results suggest the possibility of simultaneously obtaining functional and molecular information on antiangiogenic activity with targeted BR55.

However, because BR55 shows a longer blood half-life than BR1, we concluded that an additional comparison with BR38 was necessary. Furthermore, the gas phase of BR55 and BR38 is composed of a mixture of perfluorobutane and nitrogen, whereas BR1 microbubbles are stabilized with sulfur hexafluoride.

However, for the functional examination we did not perform a direct head-to-head comparison between the agents, which would be required to get hard numbers about sensitivity and specificity. A head-to-head comparison in turn requires their reference to a standard of reference measurement in the same mice (eg microvessel density as determined with histologic examination), which was not available except at the last time point. Another limitation of our study is that the comparison of molecularly targeted and nontargeted microbubbles was only performed in one tumor model and with one antiangiogenic agent. Thus, comparative analyses in additional tumor models, and with further antiangiogenic agents, is required to generalize our conclusions. In addition, two-dimensional US was performed to depict a single tumor plane. In a future study, three-dimensional measurements recording the whole tumor should also be obtained. A further limitation of our study is that the order of microbubble injection was based on the circulation time of each microbubble type and was not randomized. This was done to keep the time of anesthesia for the animals as short as possible. This is reasonable to prevent unwanted animal loss in studies with repetitive US examinations. However, it should be noted that repetitive microbubble injections might influence and reduce the regional blood flow in tumors after the application of a destructive pulse (32,33). In the choice of microbubble dosages we followed the manufacturer’s recommendations, which are different between the microbubble types

because acoustic properties and blood half-lives of the microbubbles are not identical. However, in particular for the functional first-pass analysis, dose optimization may further improve the assessment of therapy effects for one or the other microbubble type.

Furthermore, in our study, the first US measurements were performed 4 days after therapy onset. In future experiments, it would be of interest to also examine changes in US imaging signal at very early time points after the start of therapy to determine whether significant changes in US imaging signal are detectable in HaCaT-ras A-5RT3 tumors at such time points, as described, for example, by Pysz *et al.* (20) for LS174T tumors.

In summary, our results show that molecular US with VEGFR2-targeted BR55 depicts antiangiogenic therapy effects earlier than functional US imaging with nontargeted microbubbles. In addition, we showed that the functional results about tumor vascularization obtained with first-pass kinetics of BR55 werecomparable to those with nonspecific US contrast agents. Because clinical studies with nontargeted microbubbles already proved the value of dynamic contrast-enhanced US for predicting and monitoring the efficacy of antiangiogenic tumor treatment (34–36), the evaluation of BR55 for functional and molecular tumor therapy monitoring in a one-stop shop may be a logical next step.

Acknowledgments

We thank Lars Eijssen, PhD, Department of Bioinformatics, Maastricht University, for his outstanding help and support with the statistical analysis and revision. Furthermore, we thank Bracco Suisse SA (Geneva, Switzerland) for providing the microbubbles and Merck Serono (Darmstadt, Germany) for providing the anti-VEGF antibody.

Funding: This work has been supported by the European Research Council (ERC Starting Grant 309495: NeoNaNo) and by the project “ForSaTum” (cofunded by the European Union (European Regional Development Fund - Investing in your future) and the German federal state North Rhine-Westphalia (NRW).

References

1. Kiefer F, Siekmann AF. The role of chemokines and their receptors in angiogenesis. Cell Mol Life Sci. 2011; 68:2811–2830. [PubMed: 21479594]
2. Rossi D, Zlotnik A. The biology of chemokines and their receptors. Annu Rev Immunol. 2000; 18:217–242. [PubMed: 10837058]
3. Carmeliet P, Jain RK. Angiogenesis in cancer and other diseases. Nature. 2000; 407(6801):249–257. [PubMed: 11001068]
4. Romagnani P, Lasagni L, Annunziato F, Serio M, Romagnani S. CXC chemokines: the regulatory link between inflammation and angiogenesis. Trends Immunol. 2004; 25(4):201–209. [PubMed: 15039047]
5. Hanahan D, Weinberg RA. Hallmarks of cancer: the next generation. Cell. 2011; 144(5):646–674. [PubMed: 21376230]
6. Bergers G, Benjamin LE. Tumorigenesis and the angiogenic switch. Nat Rev Cancer. 2003; 3:401–410. [PubMed: 12778130]
7. Shibuya M. Differential roles of vascular endothelial growth factor receptor-1 and receptor-2 in angiogenesis. J Biochem Mol Biol. 2006; 39:469–478. [PubMed: 17002866]
8. Carmeliet P, Jain RK. Principles and mechanisms of vessel normalization for cancer and other angiogenic diseases. Nat Rev Drug Discov. 2011; 10(6):417–427. [PubMed: 21629292]
9. Hicklin DJ, Ellis LM. Role of the vascular endothelial growth factor pathway in tumor growth and angiogenesis. J Clin Oncol. 2005; 23:1011–1027. [PubMed: 15585754]

10. Deshpande N, Ren Y, Foygel K, Rosenberg J, Willmann JK. Tumor angiogenic marker expression levels during tumor growth: longitudinal assessment with molecularly targeted microbubbles and US imaging. Radiology. 2011; 258:804–811. [PubMed: 21339349]
11. Kiessling F, Huppert J, Palmowski M. Functional and molecular ultrasound imaging: concepts and contrast agents. Curr Med Chem. 2009; 16(5):627–642. [PubMed: 19199927]
12. Pochon S, Tardy I, Bussant P, et al. BR55: a lipopeptide-based VEGFR2-targeted ultrasound contrast agent for molecular imaging of angiogenesis. Invest Radiol. 2010; 45:89–95. [PubMed: 20027118]
13. Lindner JR. Microbubbles in medical imaging: current applications and future directions. Nat Rev Drug Discov. 2004; 3(6):527–532. [PubMed: 15173842]
14. Willmann JK, Paulmurugan R, Chen K, et al. US imaging of tumor angiogenesis with microbubbles targeted to vascular endothelial growth factor receptor type 2 in mice. Radiology. 2008; 246:508–518. [PubMed: 18180339]
15. Korpanty G, Carbon JG, Grayburn PA, Fleming JB, Brekken RA. Monitoring response to anticancer therapy by targeting microbubbles to tumor vasculature. Clin Cancer Res. 2007; 13:323–330. [PubMed: 17200371]
16. Lyshchik A, Fleischer AC, Huamani J, Hallahan DE, Brissova M, Gore JC. Molecular imaging of vascular endothelial growth factor receptor 2 expression using targeted contrast- enhanced high-frequency ultrasonography. J Ultrasound Med. 2007; 26:1575–1586. [PubMed: 17957052]
17. Willmann JK, Lutz AM, Paulmurugan R, et al. Dual-targeted contrast agent for US assessment of tumor angiogenesis in vivo. Radiology. 2008; 248:936–944. [PubMed: 18710985]
18. Palmowski M, Huppert J, Ladewig G, et al. Molecular profiling of angiogenesis with targeted ultrasound imaging: early assessment of antiangiogenic therapy effects. Mol Cancer Ther. 2008; 7(1):101–109. [PubMed: 18202013]
19. Tardy I, Pochon S, Theraulaz M, et al. Ultrasound molecular imaging of VEGFR2 in a rat Prostate tumor model using BR55. Invest Radiol. 2010; 45:573–578. [PubMed: 20808233]
20. Pysz MA, Foygel K, Rosenberg J, Gambhir SS, Schneider M, Willmann JK. Antiangiogenic cancer therapy: monitoring with molecular US and a clinically translatable contrast agent (BR55). Radiology. 2010; 256:519–527. [PubMed: 20515975]
21. Kiessling F. Science to practice: the dawn of molecular US imaging for clinical cancer imaging. Radiology. 2010; 256(2):331–333. [PubMed: 20656826]
22. Schneider M, Anantharam B, Arditi M, et al. BR38, a new ultrasound blood pool agent. Invest Radiol. 2011; 46(8):486–494. [PubMed: 21487303]
23. Bzyl J, Lederle W, Rix A, et al. Molecular and functional ultrasound imaging in differently aggressive breast cancer xenografts using two novel ultrasound contrast agents (BR55 and BR38). Eur Radiol. 2011; 21:1988–1995. [PubMed: 21562807]
24. Gremse F, Doleschel D, Zafarnia S, et al. Hybrid μCT-FMT imaging and image analysis. J Vis Exp. 2015; doi: 10.3791/52770
25. Palmowski M, Lederle W, Gaetjens J, et al. Comparison of conventional time-intensity curves vs. maximum intensity over time for post-processing of dynamic contrast-enhanced ultrasound. Eur J Radiol. 2010; 75:e149–e153. [PubMed: 19945241]
26. Lederle W, Hartenstein B, Meides A, et al. MMP13 as a stromal mediator in controlling persistent angiogenesis in skin carcinoma. Carcinogenesis. 2010; 31(7):1175–1184. [PubMed: 19892798]
27. Bzyl J, Palmowski M, Rix A, et al. The high angiogenic activity in very early breast cancer enables reliable imaging with VEGFR2-targeted microbubbles (BR55). Eur Radiol. 2013; 23:468–475. [PubMed: 22878592]
28. Grouls C, Hatting M, Rix A, et al. Liver Dysplasia: US Molecular Imaging with Targeted Contrast Agent Enables Early Assessment. Radiology. 2013; 267(2):487–495. [PubMed: 23360735]
29. Bachawal SV, Jensen KC, Lutz AM, et al. Earlier Detection of Breast Cancer with Ultrasound Molecular Imaging in a Transgenic Mouse Model. Cancer Res. 2013; 73(6):1689–1698. [PubMed: 23328585]
30. Lederle W, Arns S, Rix A, et al. Failure of annexin-based apoptosis imaging in the assessment of antiangiogenic therapy effects. EJNMMI Res. 2011; 1(1):26. [PubMed: 22214377]

31. Vaupel P, Kallinowski F, Okunieff P. Blood flow, oxygen and nutrient supply, and metabolic microenvironment of human tumors: a review. Cancer Res. 1989; 49:6449–6465. [PubMed: 2684393]

32. Hu X, Kheirolomoom A, Mahakian LM, et al. Insonation of targeted microbubbles produces regions of reduced blood flow within tumor vasculature. Invest Radiol. 2012; 47(7):398–405. [PubMed: 22659591]

33. Rix A, Palmowski M, Gremse F, et al. Influence of repetitive contrast agent injections on functional and molecular ultrasound measurements. Ultrasound Med Biol. 2014; 40(10):2468–75. [PubMed: 25023096]

34. Lassau N, Koscielny S, Albiges L, et al. Metastatic Renal Cell Carcinoma Treated with Sunitinib: Early Evaluation of Treatment Response Using Dynamic Contrast-Enhanced Ultrasonography. Clin Cancer Res. 2010; 16(4):1216–1225. [PubMed: 20145174]

35. Lassau N, Koscielny S, Chami L, et al. Advanced Hepatocellular Carcinoma: Early Evaluation of Response to Bevacizumab Therapy at Dynamic Contrast-enhanced US with Quantification-Preliminary Results. Radiology. 2011; 258(1):291–300. [PubMed: 20980447]

36. Lassau N, Chami L, Koscielny S, et al. Quantitative functional imaging by Dynamic Contrast Enhanced Ultrasonography (DCE-US) in GIST patients treated with masatinib. Invest New Drugs. 2012; 30:765–771. [PubMed: 21136137]

Advances in Knowledge

- Molecularly targeted ultrasound imaging with clinically translatable, vascular endothelial growth factor receptor type 2 (VEGFR2)-targeted microbubbles (BR55; Bracco, Geneva, Switzerland) depicts antiangiogenic therapy effects earlier (day 4: p=0.0058) than functional ultrasound with nontargeted BR1 and BR38 (Bracco) (day 4: p=0.4127 and p=0.6305, respectively) in a mouse xenograft model.
- First-pass data obtained with BR55 can also be used to assess vascularization, as functional information is not considerably influenced by early target binding of the microbubbles.

Implication for Patient Care

- Molecularly targeted BR55 microbubbles can be used to assess both tumor vascularization and VEGFR2 expression in tumors, thereby enabling simultaneous functional and molecularly targeted ultrasound imaging of antiangiogenic therapy responses; this encourages further clinical testing of BR55.

Europe PMC Funders Author Manuscripts

Europe PMC Funders Author Manuscripts

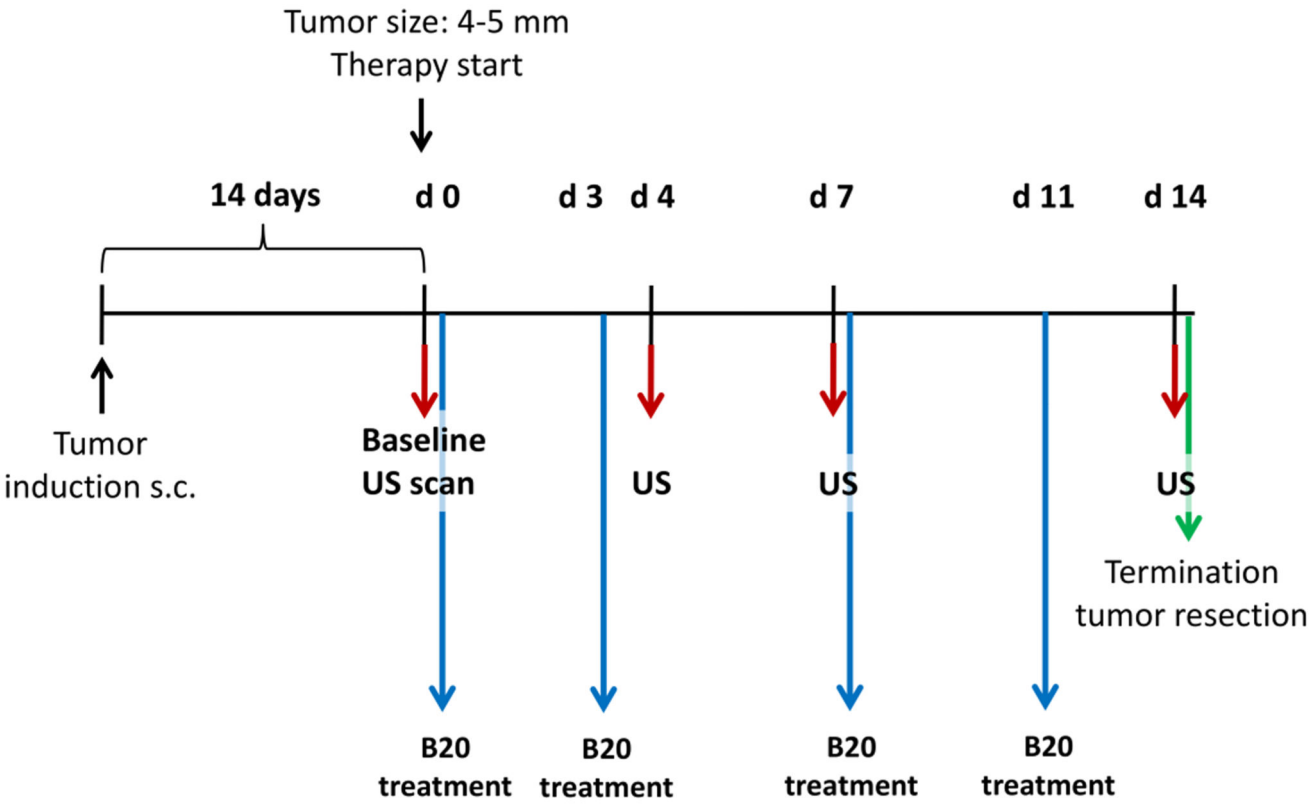

Figure 1.

Diagram of experimental study design. HaCaT-ras A-5RT3 cells were injected subcutaneously (s.c.) in right flank of nude mice. Fourteen days after tumor cell injection, baseline US was performed and mice were randomized to one of two treatment groups, receiving either B20 (n=10) or vehicle control treatment (n=10). Additional US examinations were performed 4, 7, and 14 days after therapy initiation. After the last measurement time point, mice were sacrificed and tumors were excised for histologic analysis.

Europe PMC Funders Author Manuscripts

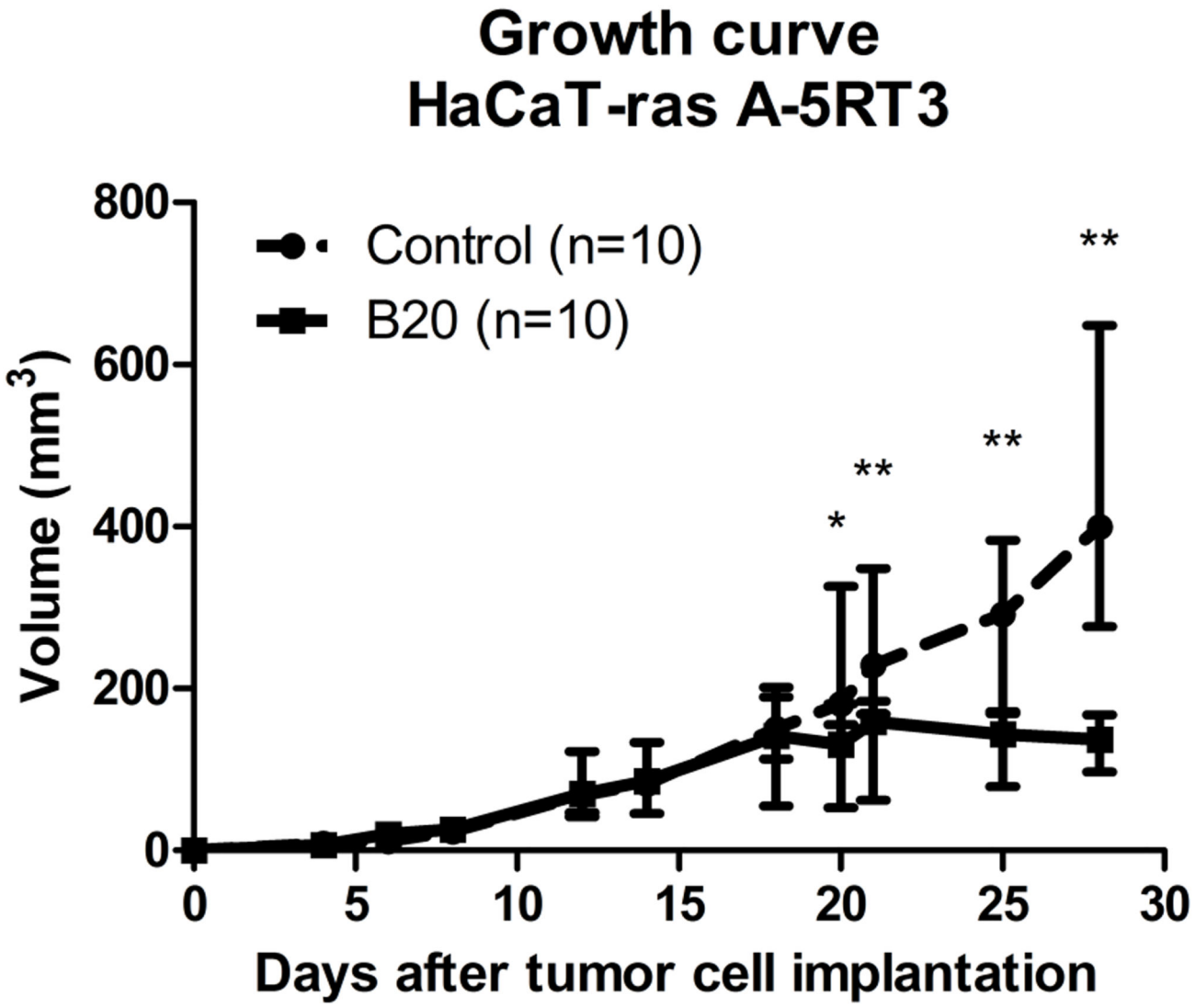

Figure 2.

Growth curve of HaCaT-ras A-5RT3 tumors in B20-treated and control animals. Therapy was started 14 days after tumor cell injection. Treatment with VEGF-antibody B20 reduced tumor growth during a 14-day period, with significant differences in tumor volume between B20-treated and control animals 6 days after treatment start (day 20). Data are medians and IQRs. * = $p < 0.05$,** = $p < 0.01$.

Europe PMC Funders Author Manuscripts

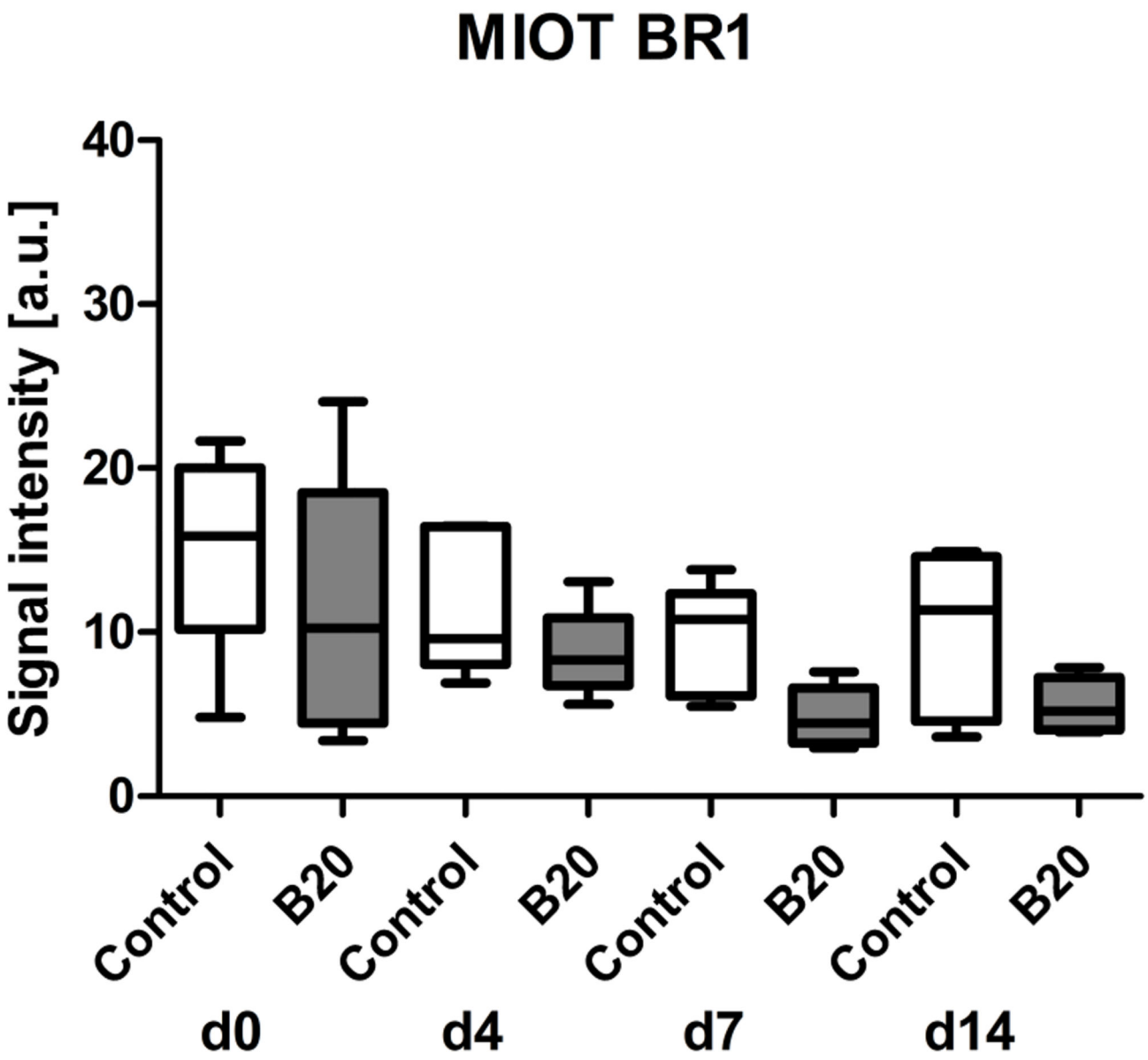

Figure 3.
Box-and-whisker plot shows analysis of rBV with postprocessing MIOT technique after injection of nontargeted BR1 microbubbles. Data are medians and IQRs.

Europe PMC Funders Author Manuscripts

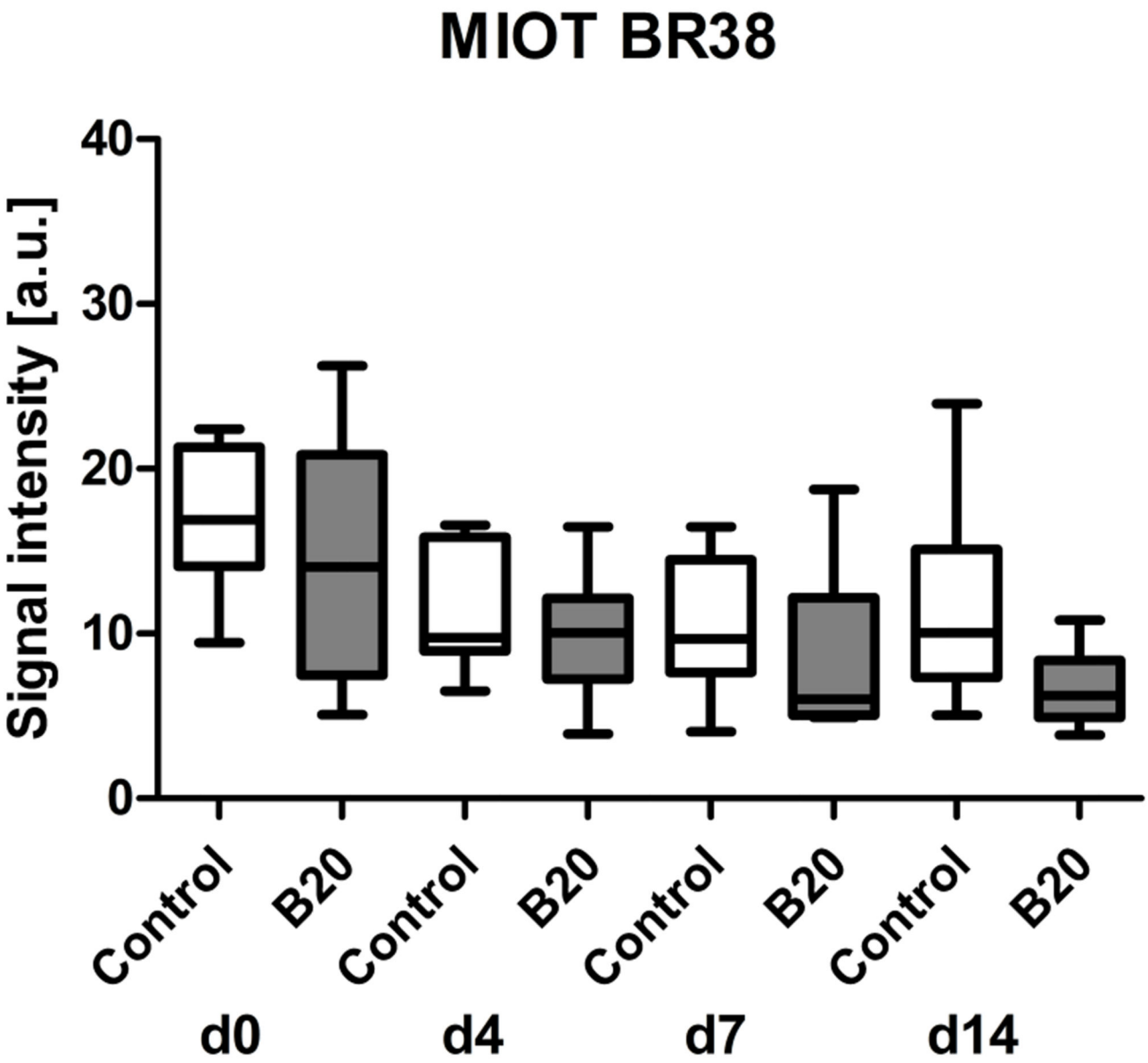

Figure 4.
Box-and-whisker plot shows analysis of rBV with postprocessing MIOT technique after injection of nontargeted, long-circulating BR38 microbubbles. Data are medians and IQRs.

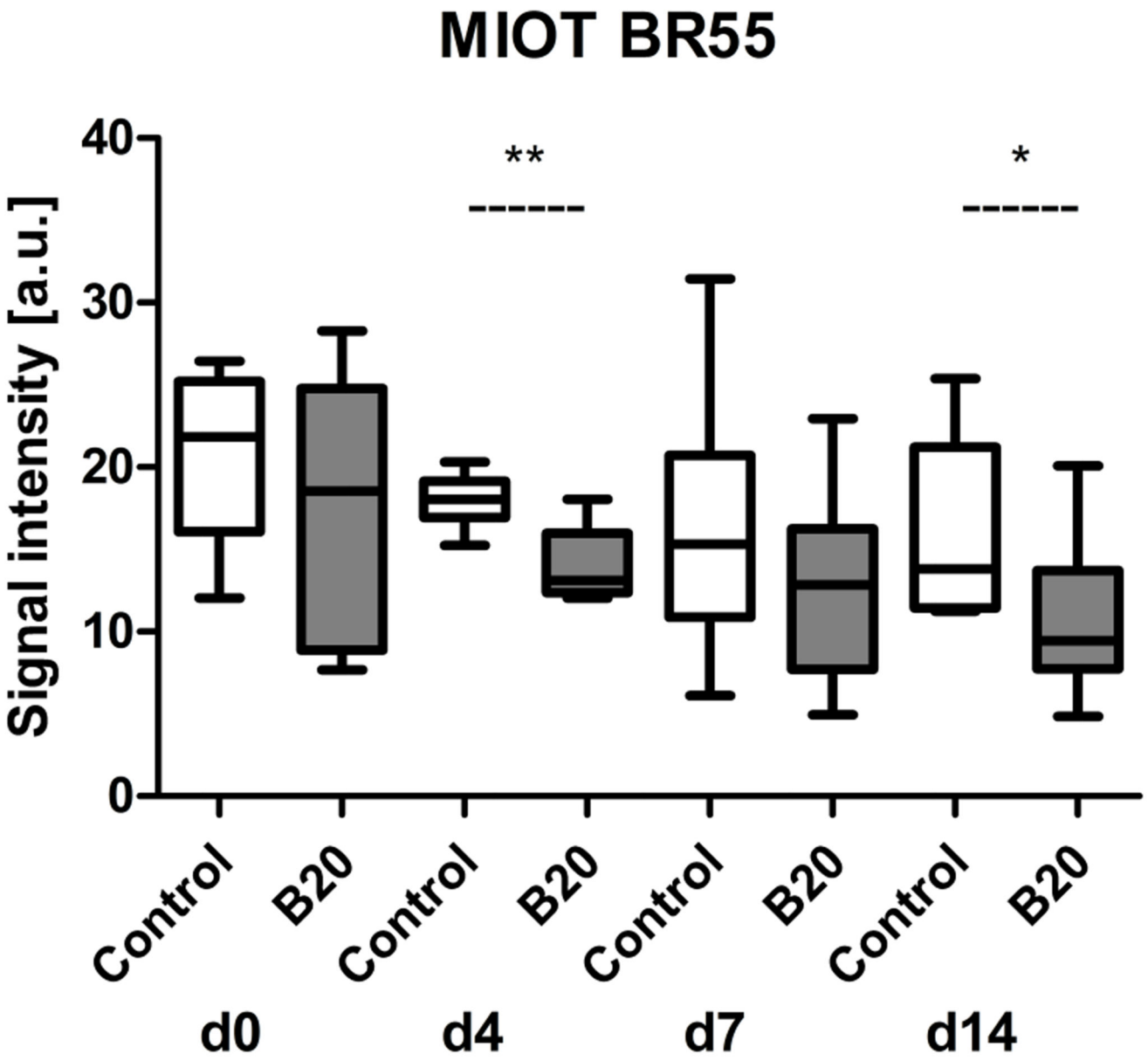

Figure 5.

Box-and-whisker plot shows results of first-pass analysis with BR55 and postprocessing with MIOT technique after injection of targeted microbubbles. Data are medians and IQRs. * = $p < 0.05$.

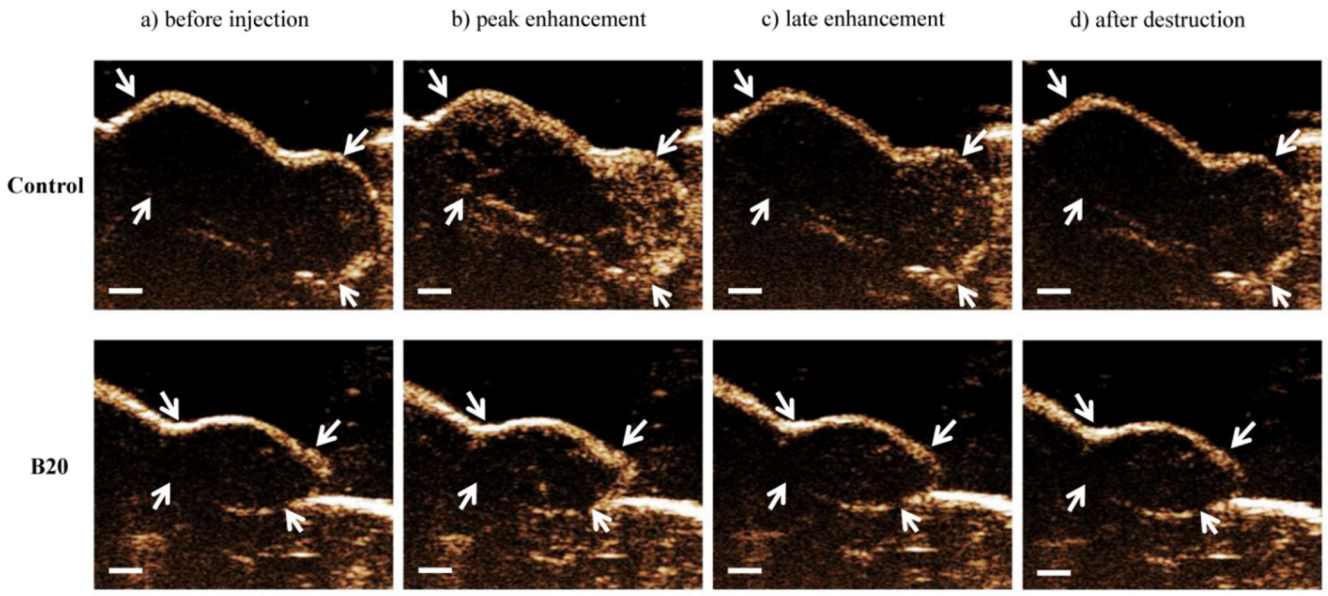

Figure 6.

Representative US images show control and B20-treated HaCaT-ras A-5RT3 tumor at therapy day 14 before and after injection of BR55 microbubbles. A higher peak enhancement is seen in control tumor compared with B20-treated tumor. Eight minutes after microbubble injection (late enhancement), the intensity of contrast enhancement is still higher in control tumor owing to bound BR55 microbubbles. Contrast intensity is markedly lower after application of a destructive pulse. Arrows indicate tumor margin. Bar = 1 mm.

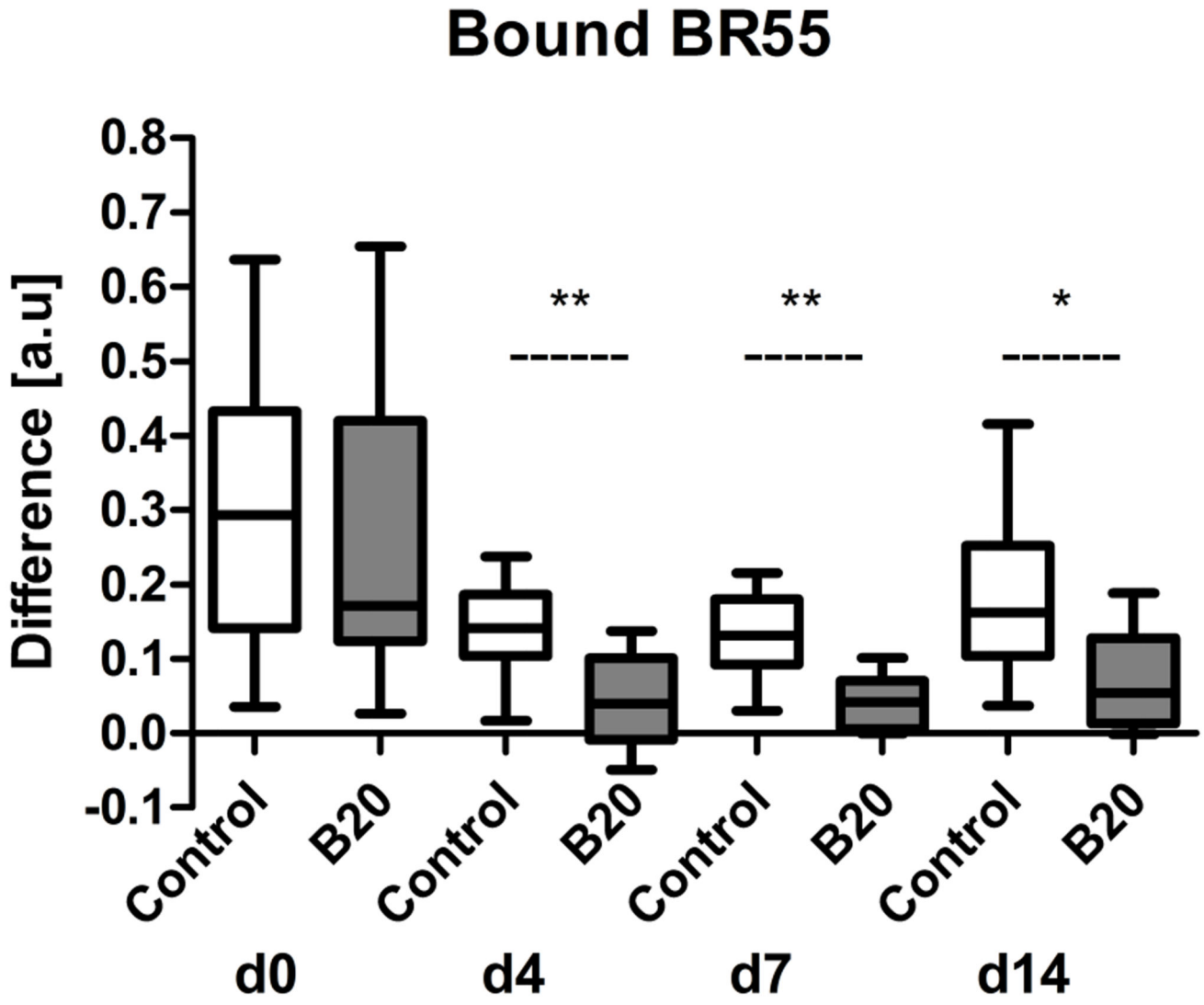

Figure 7.

Box-and-whisker plot shows amount of target-bound BR55 in B20-treated and control tumors. The amount of bound BR55 microbubbles was significantly decreased in tumors of B20-treated animals compared with control mice starting from day 4 of therapy. Results are expressed as difference in US imaging signal before and after application of a destructive pulse. Data are medians and IQRs. * = $p < 0.05$, ** = $p < 0.01$.

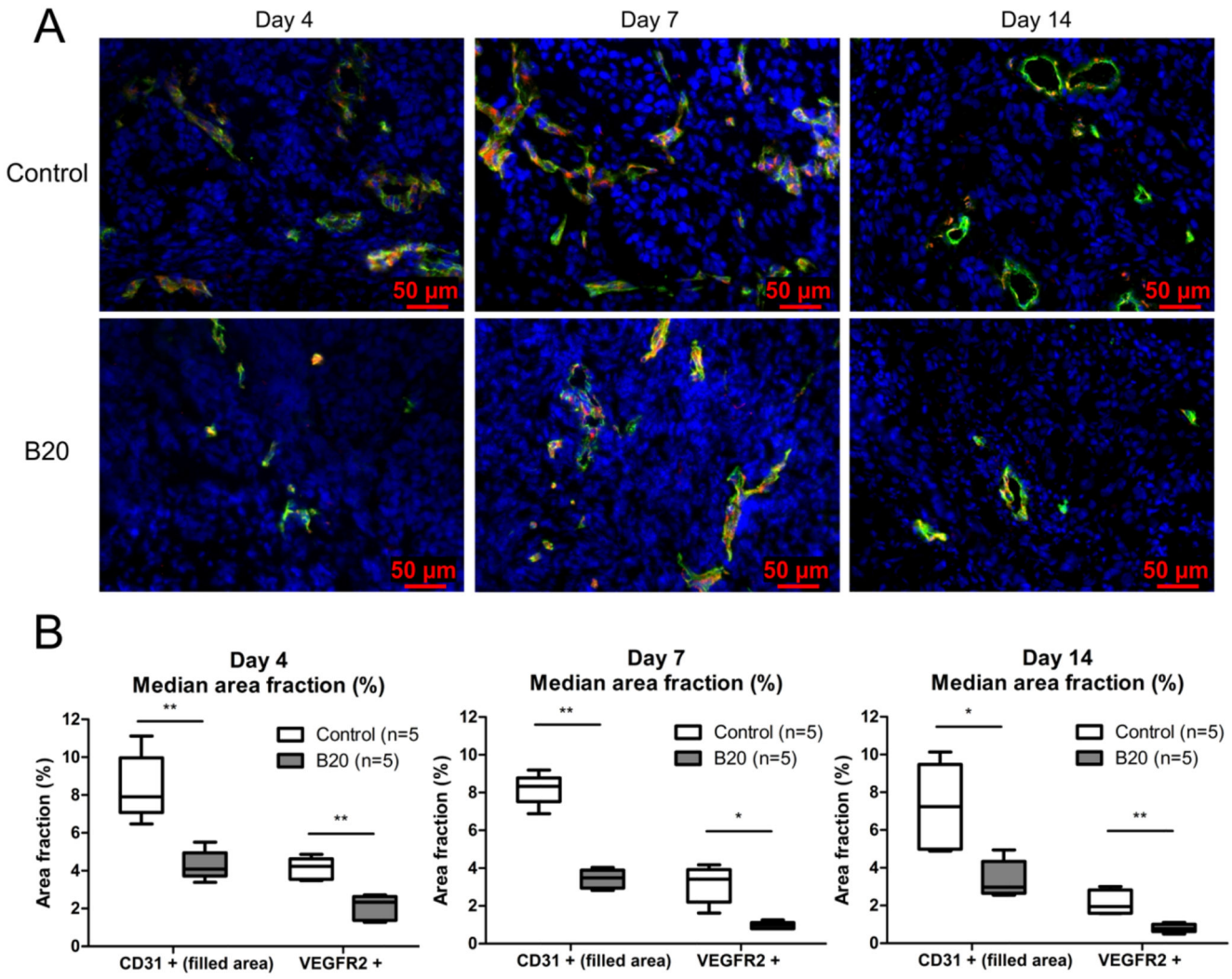

Figure 8.

Immunohistochemical analysis of microvessel density and VEGFR2 expression at treatment days 4, 7, and 14. A) Representative images for immunofluorescent staining for CD31 (green), VEGFR2 (red), and cell nuclei (blue) of control and B20-treated tumor at therapy days 4, 7, and 14. B) Box-and-whisker plots show CD31- and VEGFR2-positive area fraction at treatment days 4, 7, and 14. B20-treated tumors show a significantly decreased microvessel density and VEGFR2-positive area fraction compared with control tumors. Data are medians and IQRs. * = $p < 0.05$, ** = $p < 0.01$.

Europe PMC Funders Author Manuscripts

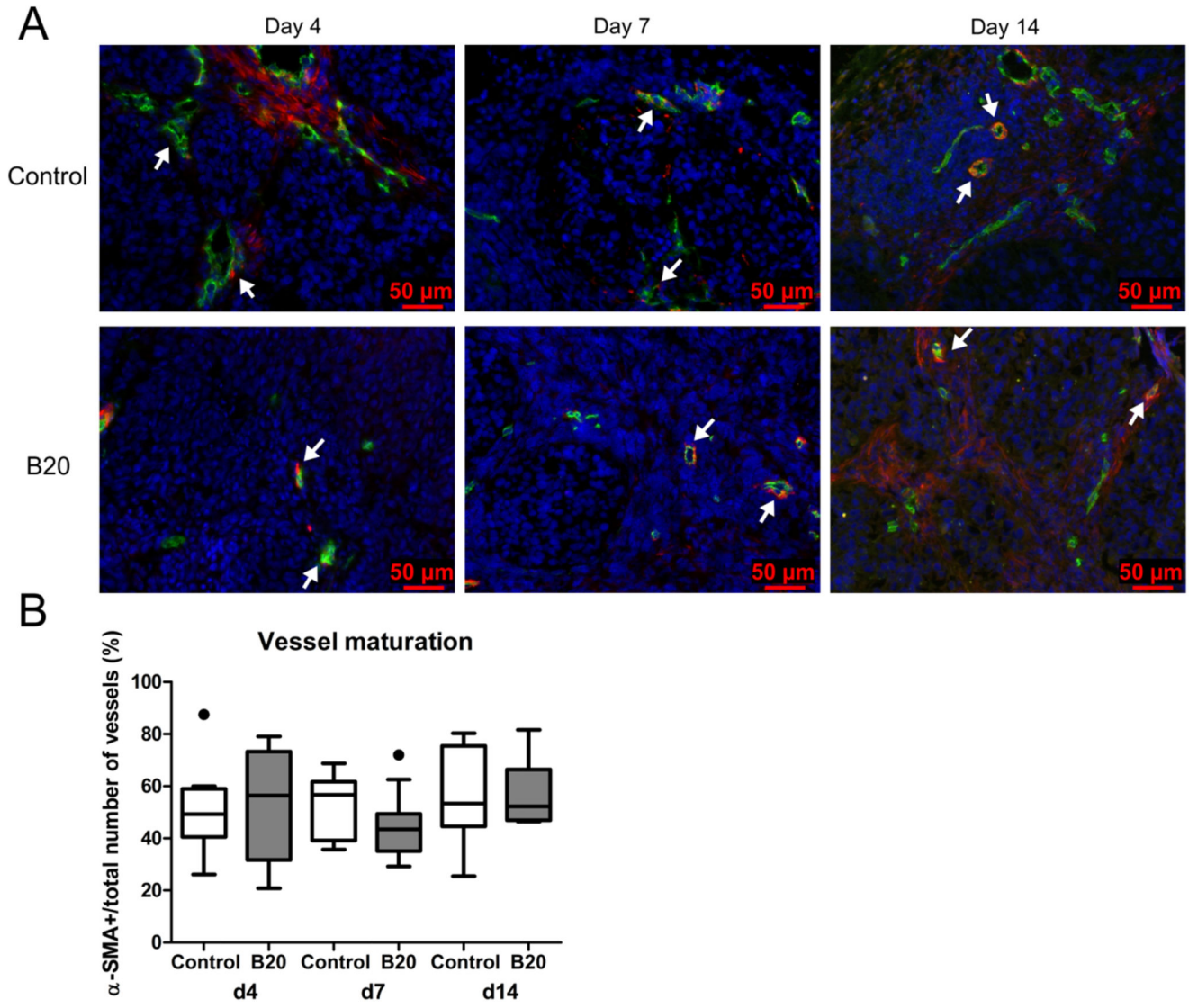

Figure 9.

Immunohistochemical analysis of vessel maturation at treatment days 4, 7, and 14. A) Images from immunofluorescent staining for CD31 (green), α-SMA (red), and cell nuclei (blue) of control and B20-treated tumor at therapy days 4, 7, and 14. Arrows indicate representative α-SMA-positive blood vessels. In addition to α-SMA-positive blood vessels, fluorescent signals from α-SMA-positive, nonvessel-associated myofibroblasts can be observed in the tumor stroma. B) Box-and-whisker plot shows median percentage of α-SMA-positive vessels. The percentage of α-SMA-positive vessels was equal for control and B20-treated tumors at therapy days 4, 7, and 14. Data are medians and IQRs. There are five tumors per experimental group. * = $p < 0.05$.